NUMERICAL INVESTIGATION ON HEAT TRANSFER, FLUID DISTRIBUTION AND SOLID STRESS TO A NEW TYPE OF SOLAR FLAT PLATE COLLECTOR

Pascal Leibbrandt, Thomas Schabbach

Institut für Regenerative Energietechnik, University of Applied Sciences Nordhausen (Germany)

Summary

For a new type of solar flat-plate collector, which is composed of planar glass plates, some of the first results of development are illustrated. In the first part of this paper the new type of flat-plate collector is introduced. A brief description of operation, heat transfer processes and radiation conversion is given. Furthermore, the advantages and disadvantages of the development in comparison to a standard flat-plate collector are discussed. In the second part simulations on heat transfer, fluid distribution and solid stress are illustrated. By using CFD (computational fluid dynamics) the aim of these first studies is to compare them to the results obtained from analytical solutions as well as an assessment of the feasibility of the concept.

Keywords: glass-collector, flat-plate collector, heat transfer, fluid distribution, solid stress

1. Introduction

Due to the stagnation of the market for solar thermal collectors in Germany since 2008 efforts are required to reduce high specific system costs ensuring the competitiveness of solar thermal systems in the future. The energy demand in Germany is due to the consumption in the heating sector over 50%. The goals of energy and climate policy can only be achieved if also solutions in the heating sector are implemented from now on. The potential of renewable energies can only be exploited if a massive build-up of new solar thermal systems is executed.

As part of the proposed research project "Nurglaskollektor" (abbreviated Nugla – means "just glass") a collector shall be developed which is composed primarily of glass, with the advantage of lower production costs.

The use of aluminum and / or copper in the absorbers increases the material- and manufacturing costs for collectors according to actual manufacturing processes. The welding and soldering of the absorber tubes and the fluid tubes is expensive with respect to the production and investment for machinery. In contrast, the Nugla collector, can be easily manufactured in an automated process. The process of manufacturing is similar to the insulating glass production. Therefore, production costs should be reduced by about 20% compared to standard flat plate collectors. The Nugla collector will have a maximum height of about 50mm, thus enabling simplified installation and connection. So, advanced application fields for solar collectors (especially in facade) are possible. Another advantage is the simplified recycling because of the construction of the collector.

2.   Construction and operation

The glass collector consists of four planar glass plates which are glued and sealed by a frame and a fluid-flow structure. As shown in fig. 1, the heat-transfer medium passes directly through the disk-space between the glasses (30) and (50). Coatings on the glass surfaces ensure optimal radiation absorption in the fluid layer and minimize the radiation losses due to reflection and emission.
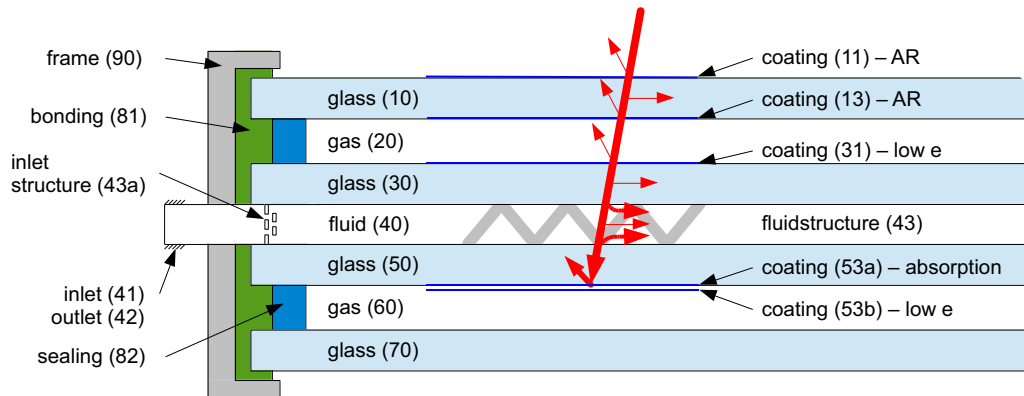

Fig. 1: Construction of the glass-collector with 4 planar glass plates, frame and coatings

The photothermal conversion is accomplished by a simple non-selective absorption layer (53a) that is located below the glass plate (50). The absorption layer (53a) is completed at the bottom by a opaque low-e layer (53b) having a low emission coefficient in the long wavelength of the radiative spectrum. The absorption layer acts upwards, the low-e layer downwards. This geometric arrangement makes the use of expensive selective coatings unnecessary. The arrangement of the functional layers (13), (31), (53a) and (53b) in the gas-filled space between the glass plates optimally protects them against environmental influence and condensation. The plane-parallel glass plates are sealed with sealings, such as polyisobutylene (82) for example, bonded with a 2-component silicone (81) and held in a form by an external aluminum frame (90). The heat transfer medium flows through a connecting port in the centrally located inlet of the collector (41) and leaves the collector on the opposite outlet (42). Through a fluid distribution device or inlet structure (43a), the heat transfer fluid is distributed on the collector width. An areal fluid-flow structure (43) forces the heat transfer fluid to a full-scale volumetric flow through the collector and thus optimize the heat transfer between the fluid and the wall.

For the assessment of the collector's efficiency a multi-dimensional stationary thermal model was created in the run-up. The resulting energy balances by modeling 34 temperature-knots are solved iteratively. The results are illustrated by the collector curves in fig. 2.
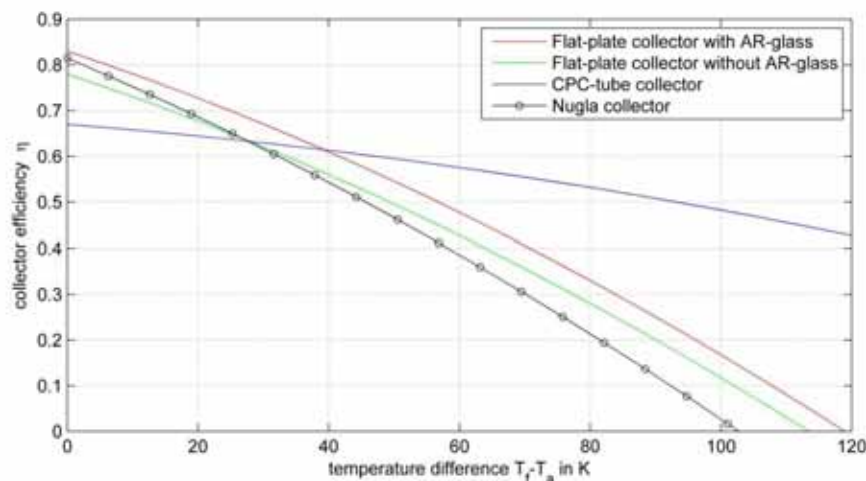

Fig. 2: Collector curves of standard collectors and the glass collector

In addition to the performance of the collector, among other things, the loads and stresses on the glasses should be estimated.

3. Numerical Investigation

To estimate the collector characteristics, fundamental numerical simulations are performed with CFD-software (CD-adapco, 2014). The software STAR-CCM+ by CD-adapco constitutes a complete simulation topology for numerical fluid mechanics, mechanical stress, heat transfer, turbulence and many more. Base on CAD to mesh via solution to post-processing and analysis, it is a complete simulation- and optimization tool.

First results relate to the investigation of the heat transfer in the gas layers (20) and (60), the fluid distribution in the fluid layer (40) and to the material stresses and deformation in the glasses according to a pressure change and/or external loads.

The simulation of heat transfer and fluid flow with CFD is based on the solution of coupled partial differential equations. The differential equations are solved iteratively by discretizing geometry in volume elements using the finite volume method. For combined calculation of forces and stress distributions, the finite element method is applied.

In the next sections, the heat transfer in the gas layers is discussed in greater detail, which is characterized by free convection. Especially the boundary layer behavior and modeling of the flow in this case lead to problems. The approaches and solutions for fluid distribution and stress analysis are briefly introduced.

3.1. Heat Transfer

The problem-setting of the heat transfer in thin gas layers with large aspect ratios is illustrated in fig. 3. Experimental correlations (Hollands, 1976) are based on temperatures of T_1 = 80°F (26.7°C), T_2 = 60°F (15.5°C) and angles of incidence between φ = 0 and 70°. A length of L = 560mm and the disk spacing of s = 12.7mm are underlying. For representations of gas flows in solar collectors, the angular range is sufficient. The maximum collector temperatures, however, are much higher and the spread may be significantly greater in high-performance solar collectors.

To check on the one hand whether the correlation by Hollands applies also to the gas flows in the new glass collector and on the other hand if CFD-simulations can be used to optimize convective heat losses, it is necessary to compare the results. In later steps the heat losses of the collector should be minimized by optimizing the glass spacing and the gas fillings.
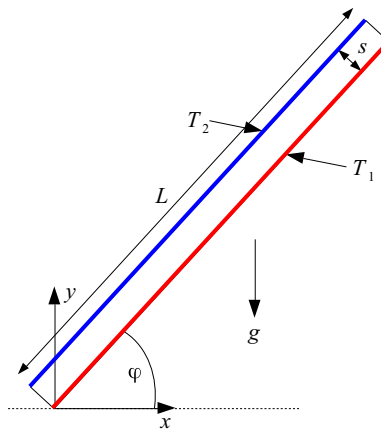

Fig. 3: Problem and geometry definition of free convective flow

The heat transfer by free convection in the gas layers was investigated by numerical simulations and comparison against experimental data (Hollands, 1976). Eq. 1 shows the correlation, which fits to the experimental data with a deviation of about 5%. The $[X]^+$ means, that only positive values of the term $[X]$ are used, zero should be used if the term is negative (Hollands, 1976).

$$Nu = 1 + 1.44 \left[1 - \frac{1708}{Ra \cdot \cos\varphi}\right]^+ \left(1 - \frac{[\sin(1.8\varphi)]^{1.6} \cdot 1708}{Ra \cdot \cos\varphi}\right) + \left[\left(\frac{Ra \cdot \cos\varphi}{5830}\right)^{1/3} - 1\right]^+ \quad \text{(eq. 1)}$$

In eq. 1 the Ra-Number is used, which is defined in this case as

$$Ra = Gr \cdot Pr = \frac{g \cdot \beta \cdot \Delta T \cdot s^3}{\nu \cdot a} \tag{eq. 2}$$

Where g is the acceleration of gravity, β the coefficient of thermal expansion, ν the kinematic viscosity, a the thermal diffusivity, ΔT the temperature difference between the plates and s the characteristic length (here the plate spacing)

Based on a simplified test-geometry as shown in fig. 3, the basic settings with respect to the discretization and the physical properties were examined. Thus, it was found that not only the discretization, the selection of the turbulence model and the boundary conditions but also the size of the gas volume are significant impacts on the simulation results. With simple settings and inappropriate boundary conditions the simulation results with respect to the heat transfer differ from the experimental data up to 15%. Comparable results also provided by the analysis of (Föste, 2013). An originally suspected reason are the different boundary conditions (temperature range 50-70°C) compared with the experimental results according to Hollands (15-26°C).

It could be shown that different boundary conditions lead to significant differences in the numerical model. In the following project steps these differences will be precisely analyzed and corrected. Not least, the experimental setup in (Hollands, 1976) deviates to the application field of solar thermal energy. For validation of the CFD-software studies are pursued by using the original boundary conditions according to (Hollands, 1976).

Fig. 4 shows some scalar temperature scenes for a heated gas volume from below for different angles of inclination. Convection rolls which arise under certain boundary conditions are visible.
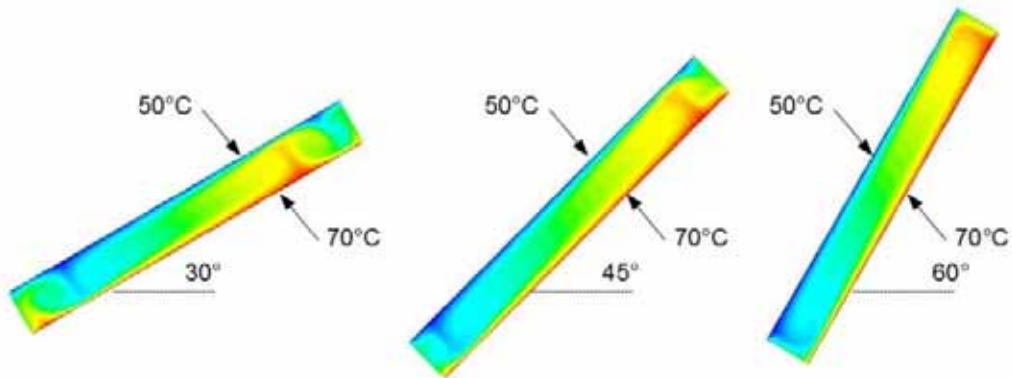

Fig. 4: Scalar Scenes Temperature for different inclination angles

Due to the high deviations between experimental data (Föste, 2013) and simulation results, a discretization convergence study was made. In this case the discretization density of the geometry is increased until there were no changes in the simulation results shown. Typically the base size of the discretization is halved each step. The base size here is the side length of a finite volume element. Further it should be noted that the discretization is based only on simple two-dimensional square elements without boundary layer discretization. The heat transfer for the test case was calculated by using (eq. 1) with s = 10mm, L = 200mm, φ = 45°, T_1 = 70°C and T_2 = 50°C, to

$$\dot{Q} = A \cdot \frac{Nu \cdot k}{s} \cdot \Delta T \tag{eq. 3}$$

The results of the convergence study are shown in tab. 1. It is obvious that a refinement of the network also leads to an increase in cell number and simulation time. A compromise has to be found between the computational effort and the expected accuracy of the results. A distinct approach of the transferred heat flux to the experimental results is unfortunately not visible even with a reduction to 1/16 of the original base size. The simulation time has, however, increased by a factor of 6000. This computational cost does not justify the minimal closer result.

Tab. 1: Results of the discretization convergence study in contrast to experimental results

Base Size in mm	Volume Cells	CPU Time in h	Heat Transfer in W	Deviation of Heat Transfer in %
-	-	-	11.23 (Experimental)	-
1.0	2,000	0.026	12.450	+ 10.86
0.5	8,000	0.420	12.300	+ 9.53
0.25	32,000	1.445	12.270	+ 9.26
0.125	128,000	19.830	12.252	+ 9.10
0.0625	512,000	164.700	12.250	+ 9.08

Visible, however, is that even coarse discretization's enable the estimation of the heat loss rate sufficiently. This in turn allows a viable simulation time with good accuracy.

It is assumed that the deviation of the results is not just based on a coarse discretization, as described above, but in the absence of boundary layer discretization. The thermal boundary layer is very important for the formation of the convective heat transfer. By the static friction condition of the wall inside the thermal boundary layer a heat transfer takes place, which is characterized essentially by heat conduction. The boundary layer consists of a wall layer and an overlying defective layer in which heat conduction and convection occur together. Only at the end of the defective layer a sufficient flow velocity exists, so that convection appears.

The modeling of the thermal boundary layer is carried out under the assumption that the transmitted heat flow by free convection must correspond to the heat flow by conduction of heat in the boundary layer. Specifications of the thermal boundary layer are shown in fig. 5. It is

$$h \cdot \left(T_1 - T\left({}^s/_2 \right) \right) = k \left. \frac{\partial T}{\partial y'} \right|_{y'=0} \tag{eq. 4}$$

By using eq. 4, the thermal boundary layer thickness δ_T can be written as:

$$\delta_T \approx \partial y' = \frac{k}{h} \tag{eq. 5}$$

In the used CFD program, the boundary layer thickness can be modeled by defining so called "Prism Layers". In this case the boundary layer thickness is donated as Prism Layer Thickness (δ_T = PLT).
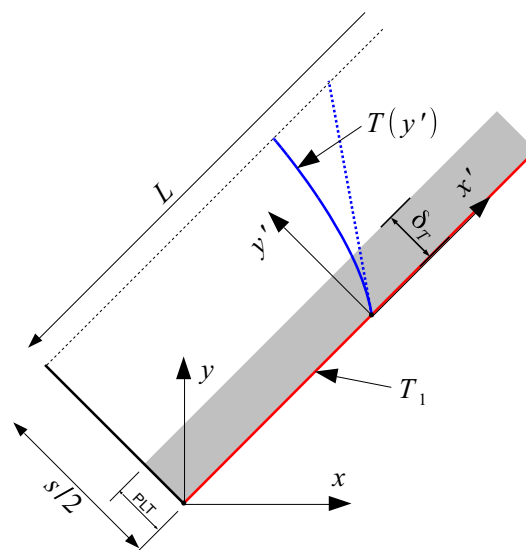

Fig. 5: Definition of Thermal Boundary Layer Thickness

In the following simulation results, two different discretization methods are compared. As shown in fig. 6, simple meshers compared with meshers including a boundary layer resolution. To compare the results the

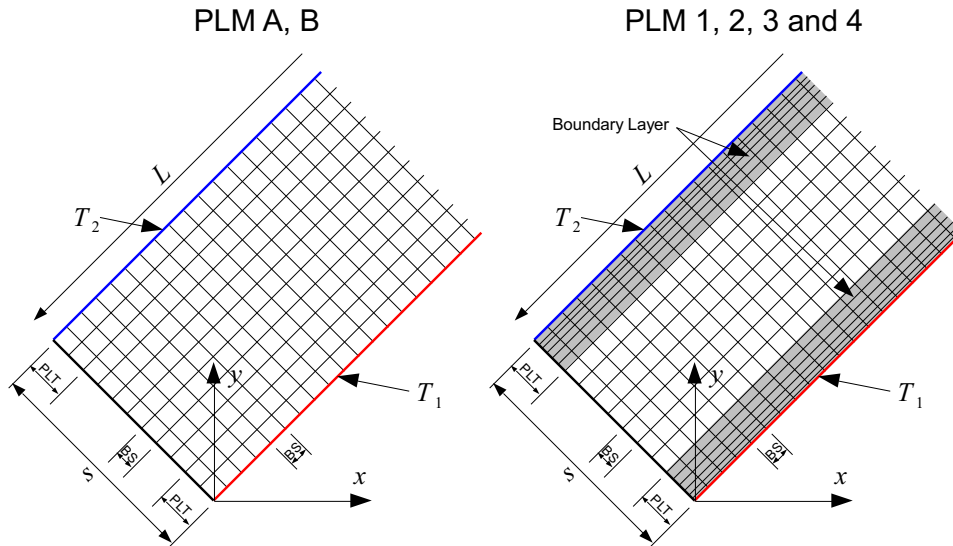base size and the settings of the boundary layer can be varied.

Fig. 6: Mesh types. Mesher PLM A, B (left). Mesher PLM1 – PLM4 with Boundary Layers (right)

As shown in tab. 2, the basic cell size and the boundary layer thickness were changed. The other variables remain unchanged. The number of Prism Layers describes how many layers are used to model the boundary layer. The Prism Layer Stretching corresponds to the ratio of the boundary layer thicknesses with the next boundary layer.

Tab. 2: Definition of Mesh Types and Mesh Results

Mesh Name	PLM A	PLM B	PLM1	PLM2	PLM4	PLM3
Base Size (BS)	1.0 mm	2.0 mm	1.0 mm	2.0 mm	1.0 mm	2.0 mm
Prism Layer Thickness (PLT)	0.0 mm	0.0 mm	2.0 mm	2.0 mm	1.0 mm	1.0 mm
Number of Prism Layers	0	0	5	5	5	5
Prism Layer Stretching	-	-	1.5	1.5	1.5	1.5
Resulting Cells	2,501,612	319,031	4,669,643	986,741	4,885,740	997,192
Accumulated Simulation Time	~ 343 h	~ 48 h	~ 392 h	~ 104 h	~ 396 h	~ 85 h

It can be seen that not only the number of cells, but also the simulation time, significantly depend on the choice of the basic size, but do not depend on the choice of Prism Layer Thickness (PLT).

For validation of the discretization (PLM A/B and PLM1 to PLM4) the simulations were carried out again modelling free convection. Notwithstanding the boundary conditions above the experimental design after (Hollands, 1976) was replicated using 3D simulations. The geometry data and boundary conditions are listed below.

- angle of incidence: $\varphi = 15\ldots75°$ (30°, 45°, 60° simulated)
- plate distance: s = 0.5in (12.7mm)
- plate area: l x b = 560x610mm ($0.34m^2$)
- temperature bottom: $T_1 = 80°F$ (26.7°C)
- temperature top: $T_2 = 60°F$ (15.5°C)

With the boundary conditions shown above, the heat transfer coefficient is between k = 1.95 and 2.24 W/m²/K and so the boundary layer thickness is between 11.1 and 12.7mm.

This means that the flow is a pure boundary layer flow. Therefore, the boundary layer discretization has a significant impact on the simulation results. In addition, it is clear that the boundary layer thickness for the given parameter range of solar collectors varies.

$$\delta_T = (T_1, T_2, \Delta T, \varphi, L, s) \tag{eq. 6}$$

Therefore different discretization settings should be made for simulations of the convective heat flows. Fig. 7 shows the influence of the discretization on the simulation result. The heat transfer is under- or overestimated depending on the cell size and the boundary layer thickness. PLM A and B is not shown because the results deviate too far from the experimental data.
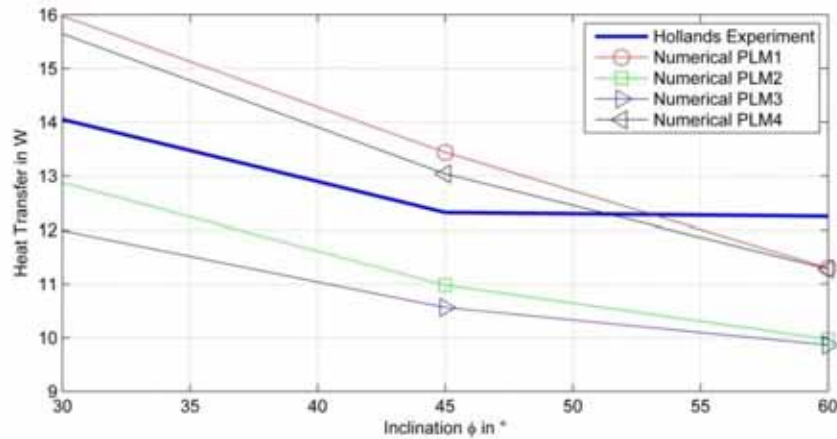

Fig. 7: Results in heat transfer for different discretization parameters

The tendency shows that the heat flow in the right order of magnitude can be predicted with CFD-simulations. The problem is the underestimation of the heat transfer for angles above 45° and the error, which is still to high, compared to the experimental correlation. Also needs to be clarified whether the formation of convection rolls in three-dimensional simulations leads to local changes in the boundary layer thickness and to what extent that affects the transferred heat flow.

The residual convergence of the simulations should be improved, too. As fig. 8 shows, the residuals seem to converge sufficiently after 10,000 iterations. The contemplation of the evaluated heat flows, however, shows a fluctuation of +/-5%.
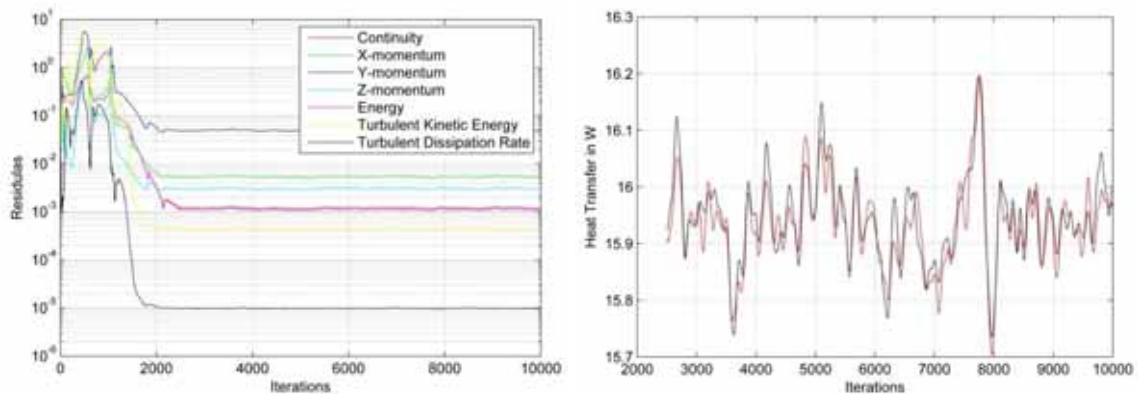

Fig. 8: Results in heat transfer for different discretization parameters

The goal of further numerical and experimental studies is thus the better adaptation of the simulation results to measured data. Based on the following study the existing correlations for free convection in closed gas layers should be adapted. So, the convective heat losses in solar thermal collectors can be modeled and minimized.

3.2. Fluid Distribution

Starting from a circular cross-section (use of standard connection elements) the heat transfer fluid should form a full volumetric flow through the fluid layer (40). A fluid flow structure ensures that after the flow distribution at the collector inlet is full volumetric. A compound of the fluid flow structure with the glasses (20) and (30) is realized, which increases the stiffness of the collector and so it's mechanical stability.

Fig. 9 shows the fluid volume in top view. The x-direction indicates the direction of flow, and the y-axis the collector width, the layer height is shown in the z-direction. The simulations were carried out with reduced dimensions. The collector area is 1412x707mm (approx. 1m^2), which will be the size of a later prototype. With the prototype, the fluid distribution will be examined by optical measurement methods.
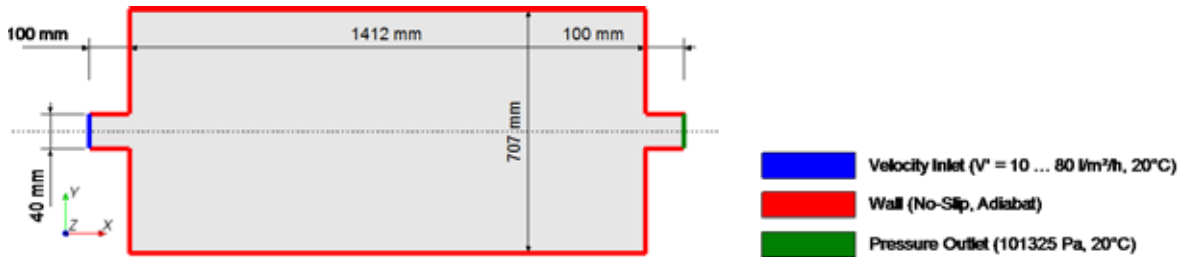

Fig. 9: Fluid layer in top view

As shown in fig. 9, modeling can be simplified in addition to the reduction to 2D simulations. So a symmetry condition is applied. The simulations were only performed for half the width of the fluid layer and then mirrored in the post-processing. For the inlet (left) face velocity and temperature have been predefined. For all walls, the static friction condition is set, the outlet pressure and temperature were determined. The simplification to a 2D simulation is set up because of the simulation time and to estimate the fluid distribution in a fast way. A real flow in the fluid layer will show a different behavior because of the boundary layer characteristics. In addition, not only the fluid distribution but also the heat transfer will be examined in later simulations.

As an evaluation criterion for the distribution of the full volumetric flow through the collector width in the flow direction, the area-weighted standard deviation of the flow velocity SSD_u was used. A_f is the discrete cell surface, $\bar{u}$ is the flow velocity averaged over the flow cross section.

$$SSD_u = \sqrt{\frac{\sum_f (u_f - \bar{u})^2 A_f}{\sum_f A_f}} \qquad \text{(eq. 7)}$$

In first 2D simulations different inlet structures are compared in terms of perfect volumetric flow and pressure loss. In later 3D simulations the heat transfer by forced convection will be evaluated as well as other criteria, too. Fig. 10 shows some of the first constructions for the in- and outlet geometry and the resulting fluid distribution.
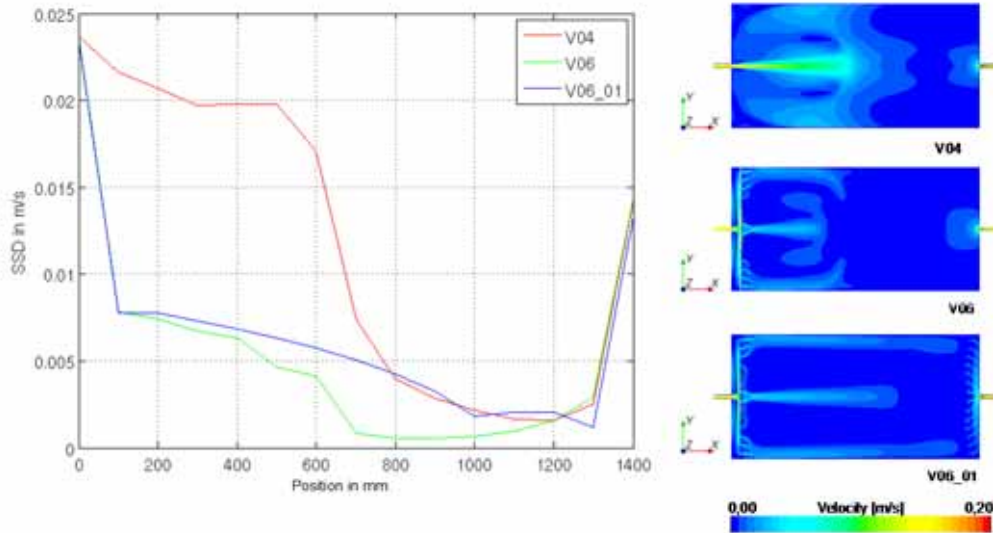
Fig. 10: Fluid distribution of the first versions

By using a grid structure after the collector inlet (V06, simple grid at the inlet) a much more uniform flow is achieved, an additional grid structure at the outlet (V06_1, simple grid at the inlet and outlet), however, does not improve the result in contrast to expectations. The flow distribution in fig. 10 on the right shows that in the center and in the side area there are still significant differences in velocity.

The improvement of the fluid distribution is done in the next steps by further comparison of alternatives (see fig. 11) and the checking of the pressure losses of the versions. Finally, the flow velocities across the collector width (y-direction) need to be modeled and tested by adjusting the pressure drop in the individual flow paths (x-direction).
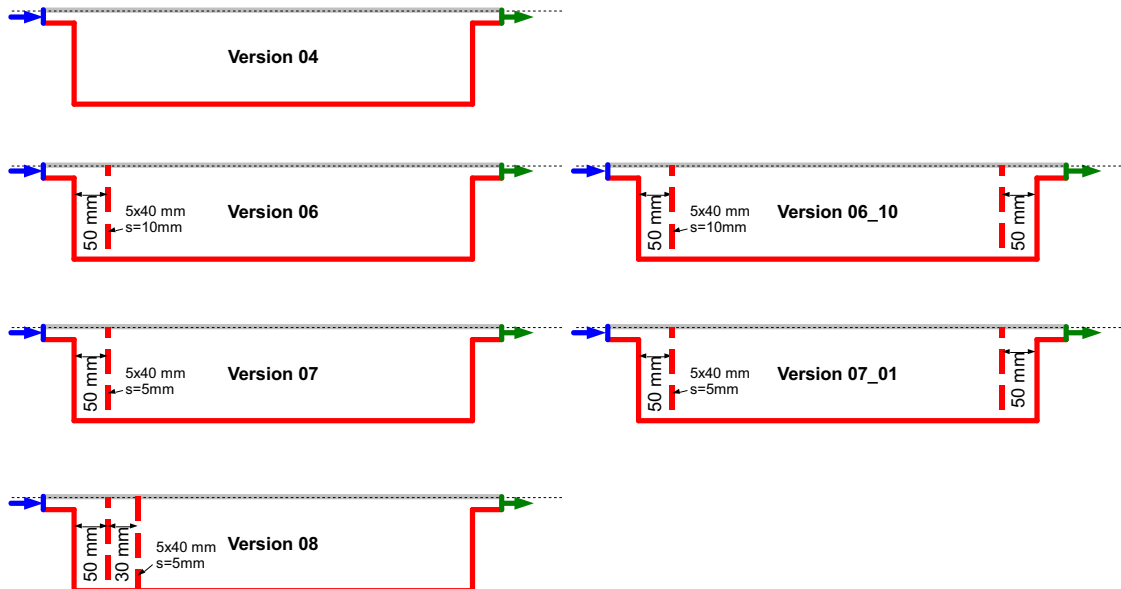

Fig. 11: Other versions for fluid distribution

3.3. Solid Stress

Starting from the calculation in the thermal model - due to internal and external loads - deformations of the glass can be expected. This makes an investigation on mechanical loads on the collector components necessary. The results shown below are not based on classical FEM simulations; instead the forces acting in the components were determined from the CFD simulations on the basis of pressure effects. In this way statements about deformations and mechanical stresses can be made.

In addition to the mechanical stresses and the bending of the glasses were analyzed by using defined loads. For this purpose, a glass plate with dimensions of 707x1412x2.4mm (W x L x T) was fixed to the side surfaces. From below a pressure of 2.0 bar (0.2 MPa) was applied.

Fig. 12 shows the results of this highly simplified structural analysis. It can be figured out that the stresses on the long side of the glass is 137MPa - the permissible stress for float glass, however, is only 18MPa in safety glass up to 45MPa. Under the given assumptions, the glass would break. The maximum deformations in the middle of the glass reach a value of about 10 mm.
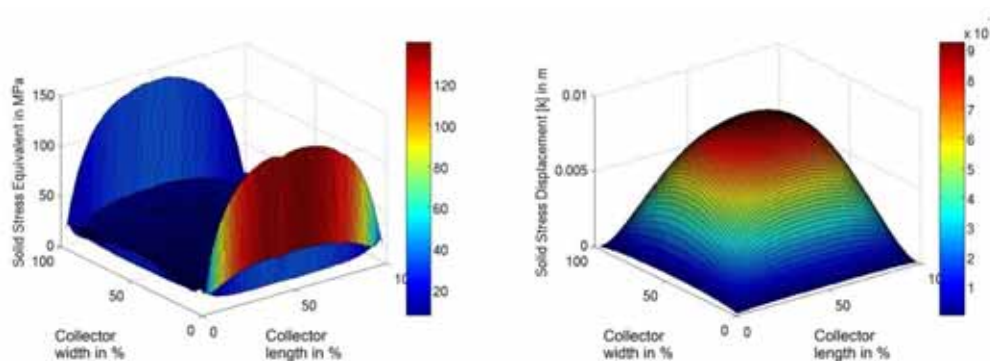

Fig. 12: Stress equivalent (left) and displacement (right) on a glass plate under a pressure of 2.0 bar

4. Outlook

In the next project parts the optimization of the in- and outlet geometry, the development of a fluid-flow-structure regarding heat transfer and pressure drop and the heat transfer in the gas layers (3D simulations) are scheduled. The assembly (distance, thickness) and functional coatings (AR, low-e, absorption) of the glass plates are examined by use of ray tracing and CFD. With a thermal model the heat losses of the edge seal, the thermal loads on glass, sealants and adhesives are modeled. Structural analysis will be done to investigate the effects of other loads (wind, snow, hail).

5. References

Hollands, K. G. T, Unny, T. E. 1976. Free Convective Heat Transfer Across Inclined Air Layers. Journal of Heat Transfer, 98, 189 – 193.

Föste, F. 2013. Flat Plate Collector with Selectively Coated Double Glazing. Leibnitz University Hanover, Doctoral Thesis.

Verein Deutscher Ingenieure. 2013. VDI-Wärmeatlas. 11. Auflage. VDI-Verlag, Düsseldorf

CD-adapco. 2014. STAR-CCM+ Version 9.02.005. http://www.cd-adapco.com